Enantioselective Inversion of a Chiral Phosphoryl Radical. A Single-Crystal ESR Analysis of X-Irradiated Bis(2,4,6-tri-*tert*-butylphenyl)phosphinic Chloride

Bas F. M. de Waal,* Olav M. Aagaard, and René A. J. Janssen

Contribution from the Laboratory of Organic Chemistry, Eindhoven University of Technology, P.O. Box 513, 5600 MB Eindhoven, The Netherlands. *Received May 13, 1991*

Abstract: ESR experiments on an X-irradiated single crystal of enantiomerically pure bis(2,4,6-tri-*tert*-butylphenyl)phosphinic chloride ($Ar_2P(O)Cl$) reveal the formation of the corresponding phosphoryl radical (**1a**, $Ar_2\dot{P}O$) via a dissociative electron-capture reaction of the PCl bond. At 120 K, this radical exhibits an exclusive and enantioselective stereoinversion in the single-crystal matrix leading to the phosphoryl radical structure **1b**. This process was monitored in detail using anisotropic ESR spectroscopy combined with X-ray crystallographic data. An analysis of the nonbonded steric interactions demonstrates that the stereoinversion is controlled intramolecularly and occurs in a synchronous reorientation of the PO bond and two methyl groups of the ortho *tert*-butyl substituents. Besides the stereoinversion, other radical reactions are observed in the crystal matrix. Ab initio quantum chemical calculations are employed to assess the electronic structure of the phosphoryl radical in more detail. An ROHF/6-31G* geometry optimization within C_s symmetry constraints yields two equilibrium structures which basically differ by their PO bond length (1.478 and 1.616 Å). The two geometries correspond to the canonical valence bond structures: $H_2\dot{P}^+-\ddot{O}^-$ and $H_2\ddot{P}-\dot{O}$, respectively. Calculated ^{31}P hyperfine interactions of the $H_2\dot{P}^+-\ddot{O}^-$ equilibrium structure are in good agreement with experiment.

Introduction

Reactions in organic molecular crystals often exhibit high regio- and stereoselectivity.[1] In contrast to the conformational freedom and random motion in solution, substrates in a molecular crystal usually possess a single spatial structure and a well-defined intermolecular orientation. The reaction pathway of a solid-state conversion is in general controlled by steric interactions of the reactant molecules with their microenvironment. This is known as "topochemical control".[2] Accordingly, a solid-state transformation proceeds with a minimal distortion of the reaction cavity formed by the surrounding stationary molecules. Several exciting examples, often photochemical in nature, have been reported, including the near-quantitative enantioselective production of permanent chirality from crystalline-phase transformations of achiral reactants.[3]

We recently demonstrated that topochemical concepts are also relevant to X-ray-induced formation of radicals in crystalline (chiral) organophosphorus compounds.[4] Following initial radical formation, the geometry relaxation, which accompanies the stabilization of a radical product from its precursor, must be accommodated in the crystal lattice. If the restraint of the environment inhibits formation of the radical configuration, which would be energetically preferred by an isolated molecule, secondary relaxation modes become accessible, leading to alternative structures.

In this paper, we report the enantioselective stereoinversion of chiral phosphoryl radicals derived from bis(2,4,6-tri-*tert*-butylphenyl)phosphinic chloride ($Ar_2P(O)Cl$, **1**, Figure 1) in a single-crystal matrix at low temperature. X-irradiation of **1** results in a dissociative electron-capture reaction giving the corresponding phosphoryl radical $Ar_2\dot{P}O$ (**1a**), via loss of Cl^- (Figure 1). The initial radical product appears to be stereochemically stable at 100 K but inverts on thermal annealing into its enantiomer (**1b**, Figure 1). The stereotransformation could be monitored in detail using the single-crystal ESR technique which provides the directional information on the orientation of the singly occupied molecular orbital (SOMO). The interconversion between the two configurations occurs in only one direction, and hence the process is enantioselective. Packing energy calculations, using X-ray crystallographic data,[5,6] are used to determine the minimum-energy path for the stereoinversion in the crystal lattice. Furthermore, we report on other reactions accompanying and following this inversion and employ ab initio quantum-chemical calculations to assess the radical configurations in more detail.

Experimental Section

X-Irradiation and ESR. Single crystals of bis(2,4,6-tri-*tert*-butylphenyl)phosphinic chloride were glued onto a quartz rod and sealed in a quartz tube. Quartz tubes containing single crystals, powdered samples, or frozen solutions were X-irradiated in a glass Dewar vessel containing liquid nitrogen (77 K) with unfiltered radiation from a Cu source operating at 40 kV and 20 mA for approximately 8 h. ESR spectra were recorded on a Bruker ER 200D spectrometer, operating with an X-band standard cavity and interfaced to a Bruker Aspect 3000 data system. In most experiments, the microwave power was set at 2 mW for optimal signal-to-noise ratio. In a typical run, a sweep width of 0.093 75 T was sampled with 4k points, resulting in a digital resolution of 0.023 mT. The single crystals were rotated perpendicular to the magnetic field from 0 to 180°, in 10° steps, with a single-axis goniometer. Temperature was controlled with the aid of a Bruker ER 4111 variable-temperature unit.

Spectral Analysis. The g values and hyperfine coupling constants of the radicals determined from the powder spectra were corrected with the Breit–Rabi equations.[7] For analysis of the single-crystal ESR spectra, we used a computer program[4c] which calculates the spin-Hamiltonian parameters from the angular dependencies of the resonant fields. For

(1) (a) Scheffer, J. R.; Garcia-Garibay, M. In *Photochemistry on Solid Surfaces*; Anpo, M., Matsiura, T., Eds.; Elsevier: Amsterdam, 1989; Chapter 9. (b) Scheffer, J. R.; Trotter, J. *Rev. Chem. Intermed.* **1988**, *9*, 271. (c) Desiraju, G. R., Ed. *Organic Solid State Chemistry*; Elsevier: Amsterdam, 1987. (d) Ramamurthy, V.; Venkatesan, K. *Chem. Rev.* **1987**, *87*, 433. (e) McBride, J. M. *Acc. Chem. Res.* **1983**, *16*, 304.

(2) Cohen, M. D.; Schmidt, G. M. J. *J. Chem. Soc.* **1964**, 1996.

(3) (a) Garcia-Garibay, M.; Scheffer, J. R.; Trotter, J.; Wireko, F. C. *Acta Crystallogr.* **1990**, *B46*, 431. (b) Hasegawa, M.; Chung, C.-M.; Muro, N.; Maekawa, Y. *J. Am. Chem. Soc.* **1990**, *112*, 5676. (c) Chen, J.; Pokkuluri, P. R.; Scheffer, J. R.; Trotter, J. *Tetrahedron Lett.* **1990**, *31*, 6803. (d) Vaida, M.; Shimon, L. J. W.; van Mil, J.; Ernst-Cabrera, K.; Addadi, L.; Leiserowitz, L.; Lahav, M. *J. Am. Chem. Soc.* **1989**, *111*, 1029. (e) Green, B. S.; Lahav, M.; Rabinovich, D. *Acc. Chem. Res.* **1979**, *12*, 191. (f) Garcia-Garibay, M.; Scheffer, J. R.; Trotter, J.; Wireko, F. C. *Tetrahedron Lett.* **1987**, *28*, 1211. (g) Cohen, M. D. *Tetrahedron* **1987**, *43*, 1211.

(4) (a) Aagaard, O. M.; Janssen, R. A. J.; de Waal, B. F. M.; Buck, H. M. *J. Am. Chem. Soc.* **1990**, *112*, 938. (b) Aagaard, O. M.; Janssen, R. A. J.; de Waal, B. F. M.; Buck, H. M. *Heteroat. Chem.* **1991**, *2*, 39. (c) Aagaard, O. M.; Janssen, R. A. J.; de Waal, B. F. M.; Kanters, J. A.; Schouten, A.; Buck, H. M. *J. Am. Chem. Soc.* **1990**, *112*, 5432.

(5) Yoshifuji, M.; Shima, I.; Inamoto, N.; Hirotsu, K.; Higuchi, T. *Angew. Chem.* **1980**, *92*, 405; *Angew. Chem., Int. Ed. Engl.* **1980**, *19*, 399.

(6) We obtained a complete list of the fractional coordinates in a personal communication from Professor M. Yoshifuji of Tohoku University, Sendai, Japan.

(7) Breit, G.; Rabi, I. I. *Phys. Rev.* **1931**, *38*, 2082.

0002-7863/91/1513-9471$02.50/0

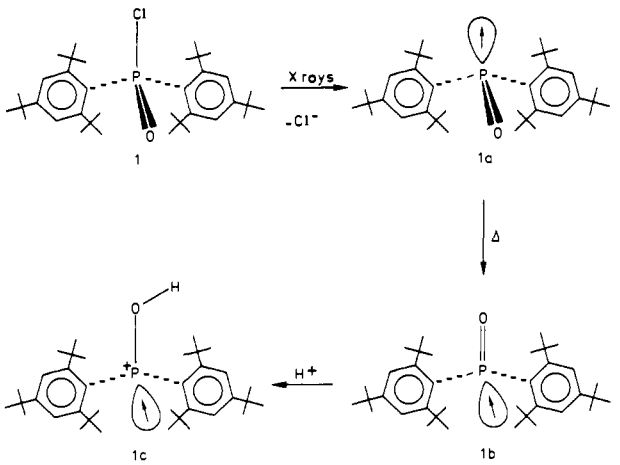

Figure 1. Structures of radicals **1a–c** formed after X-irradiation of bis(2,4,6-tri-*tert*-butylphenyl)phosphinic chloride (**1**) and subsequent annealing.

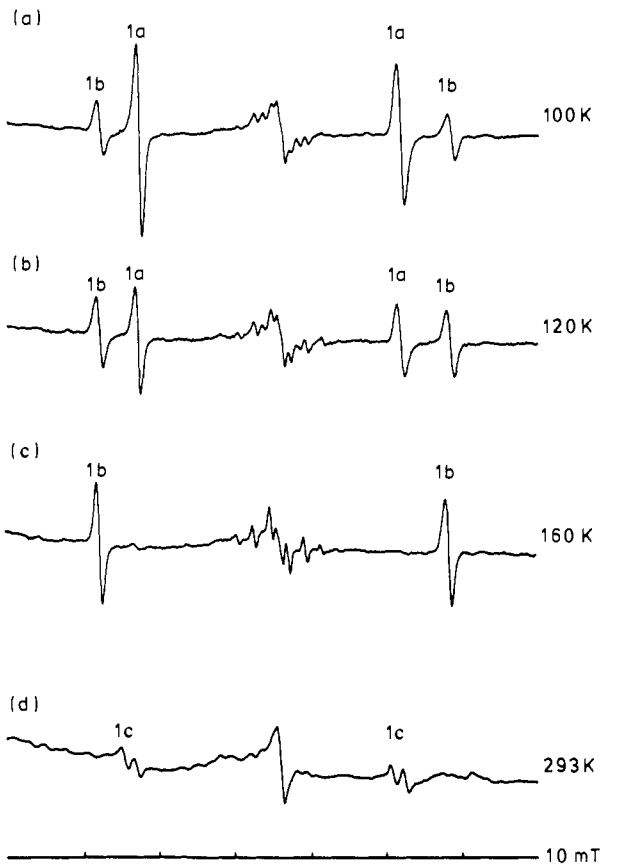

Figure 2. Single-crystal ESR spectra[10] of X-irradiated bis(2,4,6-tri-*tert*-butylphenyl)phosphinic chloride (**1**): (a) at 100 K; (b) at 120 K; (c) at 160 K; (d) at room temperature after warming to 340 K. The single crystal was aligned with the crystallographic *b* axis perpendicular to the magnetic field.

the radicals studied, the spin Hamiltonian consisted of Zeeman, nuclear Zeeman, and hyperfine parts of orthorhombic symmetry and noncoaxial orientation of **g** and **A** resulting in

$$\mathcal{H} = \beta_e \mathbf{S}\cdot\mathbf{g}\cdot\mathbf{B} - g_N\beta_N \mathbf{I}\cdot\mathbf{B} + \mathbf{S}\cdot\mathbf{A}\cdot\mathbf{I}$$

in which all symbols have their usual definition and g_N is isotropic.

Powder Spectrum Simulation. In order to reproduce the powder spectra, the **A** and **g** tensors were taken as orthorhombic and noncoincident, which is the case in the experiments. With the spin-Hamiltonian parameters derived from the single-crystal analysis, the powder spectra of the phosphorus radicals were simulated using a computer program tailored for the present spin system ($I = {}^1/_2$, $S = {}^1/_2$, and g_N isotropic) using a full diagonalization of the spin Hamiltonian.

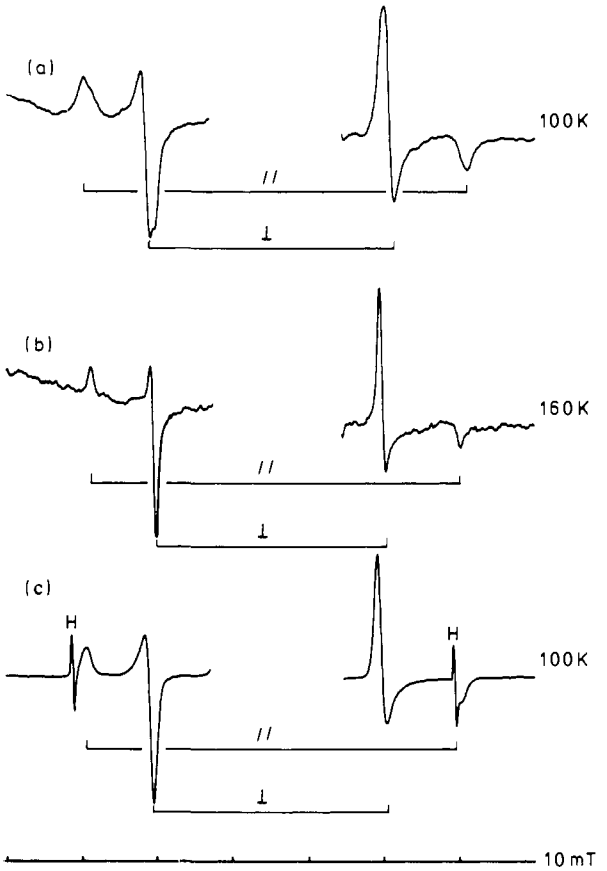

Figure 3. ESR spectra of X-irradiated bis(2,4,6-tri-*tert*-butylphenyl)-phosphinic chloride (**1**): (a) powdered sample at 100 K; (b) powdered sample at 160 K; (c) sample in a THF host matrix at 100 K. The central parts of the spectra are left out for clarity.

Bis(2,4,6-tri-*tert*-butylphenyl)phosphinic chloride (1) was synthesized from bromo-2,4,6-tri-*tert*-butylbenzene, *n*-butyllithium, and phosphoryl chloride in tetrahydrofuran according to a procedure described by Yoshifuji et al.[8,9]

Determination of the Crystal Axes. The extinction directions in the flat plane of the crystal were determined with a polarization microscope. With the rotating-crystal method using a small Debye–Scherrer camera and Cu Kα radiation, one of the extinction directions was found to correspond to the crystallographic *a* axis. The other extinction direction corresponds to the 2-fold screw axis *b*. Finally, the *c** axis of the right-handed crystal frame was defined perpendicular to *a* and *b*.

Results and Assignments

A single crystal of **1** was X-irradiated at 77 K for 8 h. The ESR spectrum of this crystal, aligned with the crystallographic *b* axis perpendicular to the magnetic field, is shown in Figure 2a. It reveals the characteristics of two phosphorus-centered radicals **1a** and **1b**. The spectrum of each radical consists of a doublet resulting from hyperfine interaction of the ^{31}P nucleus with the odd electron. At 100 K, the absorptions of **1a** are dominant (Figure 2a), but on slow thermal annealing, **1a** rapidly disappears with a concurrent increase of the signals belonging to **1b** (Figure 2b,c). At 160 K, **1a** is irreversibly lost, and the concentration of **1b** remains constant until room temperature. On subsequent heating to 340 K, **1b** disappears, and at increased gain, we detect a new phosphorus-centered radical **1c** (Figure 2d). Its double-doublet pattern is caused by a large ^{31}P interaction and a small isotropic coupling, probably from a ^1H nucleus.

The ESR spectrum of an X-irradiated powdered sample of **1** at 100 K is shown in Figure 3a. On annealing to 160 K, this

(8) Yoshifuji, M.; Shima, I.; Inamoto, N. *Tetrahedron Lett.* **1979**, *20*, 3963.

(9) Pearson, D. E.; Frazer, M. G.; Frazer, V. S.; Washburn, L. C. *Synthesis* **1976**, 621.

(10) After X-irradiation, the single crystals and powdered samples were transferred at 77 K to an unirradiated part of the sample tube in order to avoid central absorptions in the ESR spectrum due to the irradiated quartz.

Table I. Spin-Hamiltonian Parameters for Phosphoryl Radicals

radical	host	T, K		A_{iso}, MHz	$2A_{dip}$, MHz	g_{av}	ref
$Ar_2\dot{P}O$[a]	toluene	298	^{31}P	1024		2.005	12
$Ar_2\dot{P}O$[a]	cyclopropane–benzene, 1:1 (v/v)	284	^{31}P	1040		2.0030	11
			^{17}O	−26			
$Me_2\dot{P}O$	Me_3PO powder	77	^{31}P	1052	443	2.005	13
$Ph_2\dot{P}O$	$Ph_2P(O)H$ single crystal	293	^{31}P	1092	347	2.0036	14
$Ph_2\dot{P}O$	cyclopropane–benzene, 1:1 (v/v)	280	^{31}P	1013		2.0035	15
$(n\text{-Hex})_2\dot{P}O$	cyclopropane–benzene, 1:1 (v/v)	276	^{31}P	930		2.0043	15
$Ar'_2\dot{P}O$[b]	2-propanol	293	^{31}P	1044			16

[a] Ar = 2,4,6-tri-*tert*-butylphenyl. [b] Ar′ = 2,4,6-trimethylphenyl.

spectrum does not change significantly (Figure 3b), in contrast to the single-crystal spectra. Essentially due to the low concentration of **1c**, it proved to be impractiable to obtain its powder spectrum.

The ESR results indicate that **1a** and **1b** have essentially the same radical structure but are apparently differently oriented in the crystal lattice. Preliminary analysis of the powder ESR spectrum of **1a** gives the principal parallel ($A_\parallel$ = 1424 MHz) and perpendicular ($A_\perp$ = 902 MHz) parts of the hyperfine coupling tensor. The isotropic and dipolar contributions are readily obtained from the relations $A_{iso} = (A_\parallel + 2A_\perp)/3$ and $2A_{dip} = A_\parallel - A_{iso}$, resulting in 1076 and 348 MHz, respectively. On the basis of the value of A_{iso}, we assign radicals **1a** and **1b** to the bis(2,4,6-tri-*tert*-butylphenyl)phosphoryl radical $Ar_2\dot{P}O$. The same radical has previously been observed in solution, generated by hydrogen abstraction from the corresponding phosphine oxide $Ar_2P(O)H$ and originating from $Ar_2P(O)Cl$ in the presence of an electron-rich olefin.[11,12] The (isotropic) phosphorus hyperfine couplings of 1040 and 1024 MHz, respectively (Table I), are in good agreement with the present value.

Single-Crystal ESR Analysis. In order to obtain the orientations of the SOMOs of the radicals **1a** and **1b** in the crystal lattice, we performed a full single-crystal ESR analysis. Yoshifuji and coworkers have shown that single crystals of **1**, grown from *n*-pentane, belong to the chiral monoclinic space group $P2_1$ with two molecules in the unit cell at the special orientations (x, y, z) and ($\bar{x}$, $y + {}^1/_2$, $\bar{z}$). The unit cell parameters are a = 14.939 (6) Å, b = 10.924 (2) Å, c = 11.136 (4) Å, and β = 101.8 (1)°.[5] The reported phosphoryl double bond (1.684 Å) in **1** is extremely long compared to normal values (1.4–1.5 Å)[17] and even longer than PO single bonds (1.58–1.61 Å).[17c] A closer look at the molecular structure reveals that the aromatic substituents in **1** are distorted into a boat form and geometrically different. This is very likely caused by intramolecular interactions, since the complex NMR spectra reveal that even in solution the two large aryl substituents are different.[8] The strained structure is induced by the presence of four bulky *tert*-butyl groups close to the phosphorus atom.[18] This results in a chiral center on phosphorus, and consequently two enantiomeric forms of **1** exist. During crystallization, spontaneous resolution occurs, resulting in optically pure crystals.

From one single crystal, the cell parameters were redetermined using a diffractometer. The obtained cell parameters a = 14.898 (5) Å, b = 10.917 (9) Å, c = 11.111 (4) Å, and β = 101.86 (3)° are in agreement with the data of Yoshifuji and confirm that the crystal corresponds to the reported crystal structure.[5] The orientation dependencies of the ESR spectrum at 100 K in the c^*a, ab, and bc^* planes are depicted in Figure 4. In the c^*a plane, both radicals display only one orientation, since the 2-fold screw axis b is perpendicular to the magnetic field direction. Rotation in the ab and bc^* planes reveals two magnetically distinct orientations for both radicals, consistent with the crystal structure (Z = 2). The hyperfine and **g** tensors of radicals **1a** and **1b** along with their direction cosines were obtained from a computerized analysis (see Experimental Section) and are presented in Table II. For the final tensors of **1a** and **1b**, the rms error of all observed and calculated field positions is 0.21 mT, which is smaller than the line width.

Table II. Principal Values and Direction Cosines of the A (MHz) and g Tensors of Radicals **1a**(A) and **1b**(A)[a]

radical	tensor			direction cosines a	b	c^*
1a(A)	A(^{31}P)	A_1	867	−0.879	−0.384	0.283
		A_2	889	0.302	0.011	0.953
		A_3	1429	−0.369	0.923	0.106
	g	g_1	2.002	−0.091	0.972	0.216
		g_2	2.004	0.974	0.041	0.224
		g_3	2.006	−0.209	−0.231	0.950
1b(A)	A(^{31}P)	A_1	839	−0.123	0.642	0.757
		A_2	855	−0.329	−0.746	0.579
		A_3	1371	−0.936	0.178	−0.303
	g	g_1	2.003	0.870	−0.249	0.425
		g_2	2.004	−0.332	−0.934	0.132
		g_3	2.006	−0.364	0.256	0.895

[a] The direction cosines of the second orientation B are related to (a, b, c^*) by ($-a$, b, $-c^*$).

Table III. Isotropic and Dipolar Hyperfine Couplings (MHz) and Approximate Orbital Spin Densities (%) of the $Ar_2\dot{P}O$ Radicals

	radical	A_{iso}	$2A_{dip}$	ρ_s	ρ_p	p/s
single-crystal analysis	**1a**	1062	367	8.0	50.0	6.3
	1b	1022	349	7.7	47.5	6.2
powder spectrum	**1a**	1076	348	8.1	47.4	5.9
	1b	1026	351	7.7	48.0	6.2
THF spectrum		1039	360	7.8	49.0	6.3

From the single-crystal analysis, the values of the isotropic (A_{iso}) and dipolar couplings (A_{dip}) were calculated with the equations $A_{iso} = (A_1 + A_2 + A_3)/3$ and $A_{dip} = (A_3 - A_{iso})/2$ (Table III). The spin-Hamiltonian parameters of **1a** and **1b** derived from the single crystal show a close agreement with the results obtained from the powder spectra. In addition, simulation of the powder spectra using these single-crystal spin-Hamiltonian parameters reproduced the experimental spectra with high accuracy.

The present spin-Hamiltonian parameters correspond well with literature data for the same and related phosphoryl radicals (Table I) and confirm our assignment of **1a** and **1b** to different orientations of the bis(2,4,6-tri-*tert*-butylphenyl)phosphoryl radical. A_{iso} and A_{dip} give a direct measure of the phosphorus valence s- and p-orbital spin densities (ρ_s and ρ_p) of **1a** and **1b** (Table III).[19] Approximately 55–58% of the spin density is located on phosphorus with a p/s ratio of 6.3. Radical **1a** is very likely formed

(11) (a) Winter, N. J.; Fossey, J.; Beccard, B.; Berchadsky, Y.; Vila, F.; Werbelow, L.; Tordo, P. *J. Phys. Chem.* **1986**, *90*, 6749. (b) Ayant, Y.; Thevand, A.; Werbelow, L.; Tordo, P. *J. Magn. Reson.* **1987**, *72*, 251.
(12) Cetinkaya, B.; Hudson, A.; Lappert, M. F.; Goldwhite, H. *J. Chem. Soc., Chem. Commun.* **1982**, 609.
(13) Begum, A.; Symons, M. C. R. *J. Chem. Soc., Faraday Trans. 2* **1973**, *69*, 43.
(14) Geoffroy, M.; Lucken, E. A. C. *Mol. Phys.* **1971**, *22*, 257.
(15) Roberts, B. P.; Singh, K. *J. Organomet. Chem.* **1978**, *159*, 31.
(16) Baxter, J. E.; Davidson, R. S.; Hageman, H. J.; McLauchlan, K. A.; Stevens, D. G. *J. Chem. Soc., Chem. Commun.* **1987**, 73.
(17) (a) ul Haque, M. *J. Chem. Soc. B* **1970**, 934. (b) ul Haque, M. *J. Chem. Soc. B* **1970**, 938. (c) Corbridge, D. E. C. *The Structural Chemistry of Phosphorus*; Elsevier: Amsterdam, 1974.
(18) Ab initio calculations of the strain energy in this compound have been reported: Yoshifuji, M.; Shima, I.; Inamoto, N.; Aoyama, T. *Tetrahedron Lett.* **1981**, *22*, 3057.
(19) Morton, J. R.; Preston, K. F. *J. Magn. Reson.* **1978**, *30*, 577.

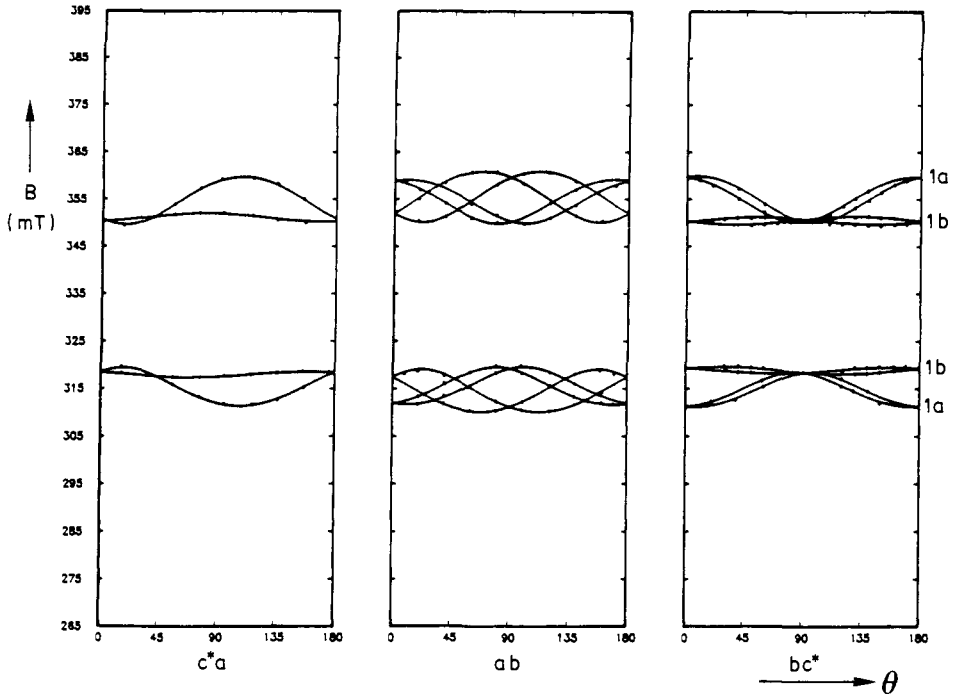

Figure 4. Angular dependencies of the resonant fields for radicals **1a** and **1b** in the c^*a, ab, and bc^* crystallographic planes.

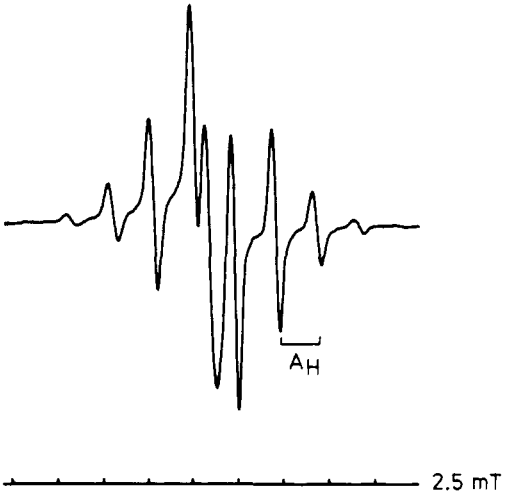

Figure 5. ESR spectrum of the *tert*-butyl radical formed after annealing of an X-irradiated sample of **1**.

by dissociative electron capture of the phosphorus–chlorine bond. Following this process, a reorientation occurs, leading to the formation of **1b**.

Concurrent with the transformation **1a** $\stackrel{\Delta}{\rightarrow}$ **1b**, thermal annealing also results in an increase of the absorptions in the central region of the spectrum. At 160 K, a well-defined 10-line pattern (Figure 5) is observed and assigned to the *tert*-butyl radical. The ^1H coupling obtained from the spectrum (63.9 MHz) is in excellent agreement with literature data (63.6 MHz).[20] The concentration of the *tert*-butyl radical increases in the same temperature trajectory as **1b**, but at present it is not clear whether these two phenomena are coupled (vide infra). At temperatures above 160 K, the *tert*-butyl radical gradually disappears and is lost from the ESR spectrum at 230 K. In addition, a large central absorption is present at 100 K, which decreases on annealing but is persistent at room temperature even after heating to 340 K (Figure 2d).

Temperature Dependence and Secondary Radical Products. In an additional experiment, we recorded the ESR spectrum of an X-irradiated single crystal of **1** aligned along the *b* axis, as a function of temperature. The temperature was varied from 100 to 160 K in regular intervals of 5 K. At every temperature, we waited 20 min before recording the ESR spectrum. At various stages during this experiment, we recooled to 100 K to check for saturation but did not observe a significant change of signal intensity with respect to the spectrum at elevated temperature.

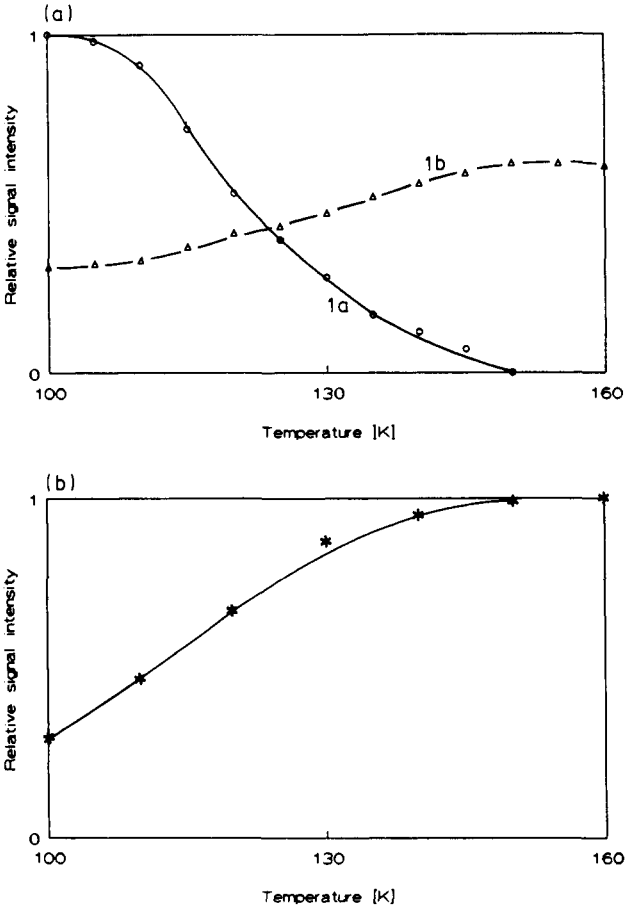

Figure 6. Relative signal intensity as a function of temperature: (a) radicals **1a** and **1b** in a single crystal; (b) the *tert*-butyl radical in a large powdered sample.

(20) (a) Krusic, P. C.; Kochi, J. K. *J. Am. Chem. Soc.* **1968**, *90*, 7155. (b) Fessenden, R. W.; Schuler, R. H. *J. Chem. Phys.* **1963**, *39*, 2147.

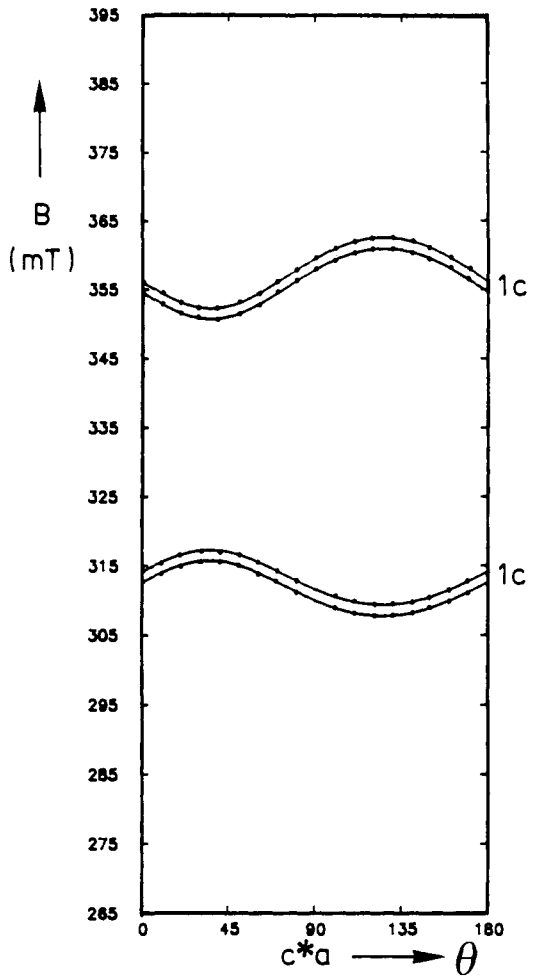

Figure 7. Angular dependence of the resonant fields for radical **1c** in the c^*a crystallographic plane.

For both radicals, the signal intensity relative to the signal intensity of **1a** at 100 K as a function of temperature is displayed in Figure 6a. This experiment reveals that **1a** disappears not only by reorientation to **1b** but also by other processes.

Eventually, after room temperature is attained, **1b** disappears, and upon subsequent warming to 340 K, extremely weak signals of a new phosphorus-centered radical **1c** appear in the spectrum (Figure 2d). Radical **1c** exhibits a large ^{31}P hyperfine interaction and an additional doublet splitting. Unfortunately, we did not succeed in performing a full single-crystal analysis of **1c**. Only one (c^*a plane) of the three independent rotation series required showed a sufficient signal-to-noise ratio for an unambiguous spectral assignment. From the angular dependence, however, it is clear that the anisotropy of **1c** (Figure 7) closely resembles that of **1b** (Figure 4). Consequently, we assign **1c** to the $Ar_2\dot{P}OH^+$ radical formed by hydrogen uptake of the phosphoryl oxygen of **1b**. The additional $I = {}^1/_2$ splitting is assigned to the interaction of the hydroxyl proton with the unpaired electron. The observed, nearly isotropic ^1H coupling of 45–48 MHz for **1c** is in accordance with the value for the related $Ph\dot{P}(O)OH$ radical ($A_\parallel$ = 49, $A_\perp$ = 42 MHz).[21]

Concurrent with the initial transformation **1a** $\stackrel{\Delta}{\rightarrow}$ **1b**, thermal annealing also results in the formation of *tert*-butyl radicals. Analogous to the procedure for **1a** and **1b**, we recorded the temperature dependence of the *tert*-butyl radical in a large powdered sample (Figure 6b). As mentioned previously, the increase of the *tert*-butyl radical concentration might be coupled with the simultaneous loss of **1a**. However the mechanism involved in such a process is unclear. Tordo et al.[11] determined that the decomposition of the $Ar_2\dot{P}O$ radical **1a** in solution proceeds via first-order

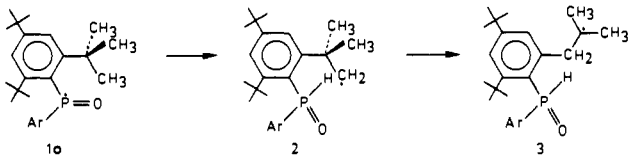

Figure 8. Mechanism proposed for the *intra*molecular proton abstraction and 1,2-aryl migration in the isomerization of **1a** into **2** and **3**.

Table IV. Fractional Coordinates of the Atoms Linked to Phosphorus for **1**[6]

atom	x	y	z
Cl	0.7116	0.6510	0.5401
P	0.7961	0.5110	0.5161
O	0.9092	0.5356	0.5614
C(1)	0.7629	0.3873	0.6139
C(7)	0.7712	0.4778	0.3487

Table V. Normalized PCl and PO Bond Vectors in Cartesian Coordinates (a, b, c^*) for the Two Molecules in the Unit Cell

		direction cosines		
molecule	bond	a	b	c^*
1	PCl(1)	−0.647	0.751	0.128
	PO(1)	0.942	0.160	0.293
2	PCl(2)	0.647	0.751	−0.128
	PO(2)	−0.942	0.160	−0.293

kinetics and presupposed an intramolecular hydrogen-abstraction reaction leading to a derivative of the 2-methyl-2-phenylpropyl radical (**2**, Figure 8). In a subsequent rearrangement reaction, a 1,2-aryl migration could in principle afford a neophyl derivative (**3**, Figure 8). Accurate ^1H hyperfine coupling parameters are known for both species, but neither of them can account for the observed 10-line spectrum.[22]

Frozen Solution. X-irradiation of a frozen solution of **1** in tetrahydrofuran (THF) also leads to the formation of the $Ar_2\dot{P}O$ radical (Figure 3c, Table III), which disappears on annealing without formation of new phosphorus radicals. The *tert*-butyl radical was not detected in the THF matrix.

Directional Analysis. The direction cosines of the maximum principal ^{31}P hyperfine coupling ($A_3(^{31}P)$) provide useful information on the direction of the phosphorus valence 3p orbital contributing to the SOMO. This results from the fact that the direction of $A_3(^{31}P)$ is identical with the direction of the 3p orbital. It is tempting to match the single-crystal ESR data of **1a** and **1b** to the orientation of the undamaged molecules using the crystal structure data (Tables IV and V). However, an unambiguous correlation of the molecular frame and the ^{31}P hyperfine tensors is not possible due to the 2-fold crystallographic symmetry. As a consequence of the two molecules (1 and 2) in the unit cell, two orientations (A and B) for both **1a** and **1b** are generated, and it is not trivial how they are related. In principle, four different assignments can be envisaged:

$$\begin{aligned} &\text{molecule 1} \xrightarrow{\text{X-rays}} \mathbf{1a(A)} \xrightarrow{\Delta} \mathbf{1b(A)} \\ &\text{molecule 2} \xrightarrow{\text{X-rays}} \mathbf{1a(B)} \xrightarrow{\Delta} \mathbf{1b(B)} \end{aligned} \quad \text{(I)}$$

$$\begin{aligned} &\text{molecule 1} \xrightarrow{\text{X-rays}} \mathbf{1a(A)} \xrightarrow{\Delta} \mathbf{1b(B)} \\ &\text{molecule 2} \xrightarrow{\text{X-rays}} \mathbf{1a(B)} \xrightarrow{\Delta} \mathbf{1b(A)} \end{aligned} \quad \text{(II)}$$

$$\begin{aligned} &\text{molecule 1} \xrightarrow{\text{X-rays}} \mathbf{1a(B)} \xrightarrow{\Delta} \mathbf{1b(B)} \\ &\text{molecule 2} \xrightarrow{\text{X-rays}} \mathbf{1a(A)} \xrightarrow{\Delta} \mathbf{1b(A)} \end{aligned} \quad \text{(III)}$$

$$\begin{aligned} &\text{molecule 1} \xrightarrow{\text{X-rays}} \mathbf{1a(B)} \xrightarrow{\Delta} \mathbf{1b(A)} \\ &\text{molecule 2} \xrightarrow{\text{X-rays}} \mathbf{1a(A)} \xrightarrow{\Delta} \mathbf{1b(B)} \end{aligned} \quad \text{(IV)}$$

(21) Geoffroy, M.; Lucken, E. A. C. *Mol. Phys.* **1972**, *24*, 335.

(22) Hamilton, E. J.; Fischer, H. *Helv. Chim. Acta* **1973**, *56*, 795.

Table VI Relative Orientations (deg) of the PCl and PO Bond Vectors of the Two Molecules in the Unit Cell and the Major Principal Couplings of the Phosphonyl Radicals **1a**(A,B) and **1b**(A,B)

	PCl(1)	PCl(2)	PO(1)	PO(2)	**1a**(A)	**1a**(B)	**1b**(A)	**1b**(B)
PCl(1)	0							
PCl(2)	82.6	0						
PO(1)	116.9	46.2	0					
PO(2)	46.2	116.9	161.6	0				
1a(A)	18.9	63.8	99.8	62.4	0			
1a(B)	63.8	18.9	62.4	99.8	45.2	0		
1b(A)	45.5	115.7	160.6	1.2	61.5	98.6	0	
1b(B)	115.7	45.5	1.2	160.6	98.6	61.5	159.5	0

The problem is now to discriminate between the various possibilities, and it is practical to calculate the mutual orientations of the PCl and PO bonds and the principal directions of $A_3(^{31}P)$ (Table VI). Because no absolute sign can be attributed to a principal direction of the hyperfine tensor, there exists an ambiguity of ±180° in the values of **1a**(A,B) and **1b**(A,B).

As mentioned before, radical **1a** is likely to be formed in a dissociative electron-capture reaction of the PCl bond. The intermediate three-electron P∴Cl σ^* structure remains undetected. Nevertheless, similar P∴Cl σ^* radicals have been observed and studies in a number of single-crystal ESR studies, giving anisotropic information. For example, in a study on the electron capture reaction of dipyrrolidinochlorophosphine sulfide, both the P∴Cl σ^* radical and its dissociation product were observed.[23] Their respective $A_3(^{31}P)$ directions are inclined by 12°. This small angle indicates a near-in-line mode of the dissociation process which can be rationalized by the elongation until cleavage of the three-electron bond due to its partial antibonding character. In addition, it was shown that the directions of the maximum principal ^{31}P and ^{35}Cl tensor elements lie in the ClPS plane of the undamaged molecule. In a related study, Geoffroy et al.[24] presented a single-crystal analysis of the P∴Cl σ^* radical derived from 1,2-phenylene phosphorochloridate. In this radical, the $A_3(^{31}P)$ and $A_3(^{35}Cl)$ directions reside in the ClPO plane. The directions of these couplings relative to the precursor molecule are unknown. The dissociation product was detected not in the crystalline matrix but only in a frozen solution from which no directional information can be obtained. Finally, we have recently shown that during X-irradiation of (2*R*,4*S*,5*R*)-2-chloro-3,4-dimethyl-5-phenyl-1,3,2-oxazaphospholidine 2-sulfide[4a] a P∴Cl σ^* radical is formed by electron capture. In this structure, $A_3(^{31}P)$ and the PCl bond of the precursor molecule are inclined by an angle of 12–17°.

All this information strongly suggests that in the present case the $A_3(^{31}P)$ direction of the dissociative electron-capture product **1a** should be close to the original PCl bond. This result is equivalent to the conclusion that upon dissociation the tetrahedral configuration of the four-coordinated phosphorus atom is essentially preserved. From Table VI, it appears that processes I and II are in accordance with this conclusion, since the initial reorientation amounts to only 18.9°, whereas the alternative reactions (III) and (IV) would imply a serious deviation of 63.8°. In addition, the deviation of **1a**(A) and the ClPO(1) plane is small (8.2°). Upon annealing, **1a** reorients to **1b**. Again the choice between the two remaining possibilities (I) and (II) cannot be made unambiguously from the experimental data. Nevertheless, there is a perfect fit of the direction of PO(1) with **1b**(B) and of PO(2) with **1b**(A) (deviation of only 1.2°) in favor of process II. The alternative, process I, which leads to a deviation of 160.6° (or 19.4°), cannot be ruled out. In addition, **1b**(A) is also close to the original ClPO(1) plane (deviation = 7.4°). It is clear that the reorientation of **1a** to **1b** involves a major rearrangement of the $A_3(^{31}P)$ direction. Depending on the actual process taking place, the rotation of $A_3(^{31}P)$ amounts to 61.5° (or 118.5°) for (I) or to 98.6° (or 81.4°) for (II). This reorientation of $A_3(^{31}P)$ does not influence the p/s ratio of the $Ar_2\dot{P}O$ phosphoryl radical, and hence a rehybridization is unlikely; i.e., **1a** and **1b** possess essentially the same electronic configuration. The possibility that one of the bulky 2,4,6-tri-*tert*-butylphenyl groups changes its position in the single crystal can be ruled out because of severe steric interactions. The most likely explanation for the transformation of **1a** into **1b** is a stereoinversion on phosphorus, schemetically depicted in Figure 1. A stereoinversion involving a translocation of the phosphoryl oxygen explains the significant reorientation and the similarity of the electronic structures and can proceed with a minimum of molecular motion in the matrix.

Electronic Structure. Recently there has been some debate in the literature concerning the electronic structure of phosphoryl radicals ($R_2\dot{P}O$). Tordo and co-workers reported the isotropic ^{31}P and ^{17}O hyperfine couplings of the $Ar_2\dot{P}O$ radical (Ar = 2,4,6-tri-*tert*-butylphenyl, Table I).[11] The negative sign of the ^{17}O coupling ($A_{iso}(O) = -26$ MHz) is associated with a positive spin density at the oxygen nucleus as a consequence of a negative g_N value for ^{17}O. This positive spin density has been interpreted as evidence for an important contribution of the $Ar_2\dot{P}$–$\dot{O}$ canonical structure to the electronic configuration. Tordo's ab initio calculations on the $H_2\dot{P}O$ prototype at the 6-31G* unrestricted Hartree–Fock (UHF) level seemed to concur with this conclusion but are open to discussion. First, the theoretical hyperfine couplings were obtained indirectly via a Mulliken atomic spin-population analysis and not from a direct evaluation of the Fermi contact integral.[25] Second, a planar geometry was imposed on $H_2\dot{P}O$. This geometry results in a C_{2v} point group which *prohibits*, by symmetry, any contribution of the phosphorus and oxygen (valence) s orbitals to the SOMO of the $^2B_1$ ground state. Consequently, the reported isotropic hyperfine couplings and valence s-orbital spin densities can only be the result of spin contamination as an artifact of the UHF theory.

In a more elaborate ab initio study, Nguyen and Ha tried to overcome some of these limitations by performing UHF, unrestricted Møller–Plesset (UMP), and configuration interaction (CI) calculations on fully optimized structures of $H_2\dot{P}O$ and $H_2\dot{P}S$.[26] However, their conclusions need to be commented on. Using the appropriate spin operator, Nguyen and Ha obtained a quantum-chemically correct estimate of the spin densities at the ^{31}P, ^{17}O, and ^{33}S nuclei. In the subsequent conversion to hyperfine coupling constants, they did not include the negative sign of the ^{17}O g_N value and consequently arrive, mistakenly, at the conclusion that their calculations fail to reproduce the negative sign of the ^{17}O coupling. The isotropic ^{31}P hyperfine coupling of 860 MHz (obtained correctly from a CISD/DZP//UMP2//6-31G** calculation) is less than the experimental value (Tables I and III) but indicates that the calculations are probably qualitatively correct. The corresponding value for the thiophosphoryl $H_2\dot{P}S$ radical is predicted to be only half of that of its phosphoryl analogue. Although unmentioned, this is in contrast with experimental evidence.[27,28]

In our opinion, some of the obscurities and discrepancies encountered can be solved by examining the anisotropic (dipolar) hyperfine coupling, which is known experimentally and can also be obtained from ab initio calculations. The present single-crystal ESR analysis reveals large (349–367 MHz) dipolar hyperfine couplings (Table III), pointing to an important contribution (≈ 50%) of the phosphorus 3p orbital to the SOMO of $Ar_2\dot{P}O$. To

(23) Janssen, R. A. J.; Sonnemans, M. H. W.; Buck, H. M. *J. Am. Chem. Soc.* **1986**, *108*, 6145.

(24) Cattani-Lorente, M.; Bernardinelli, G.; Geoffroy, M. *Helv. Chim. Acta* **1987**, *70*, 1897.

(25) The Mulliken population analysis revealed $\rho_s(P) = 0.106$ and $\rho_s(O) = 0.0089$, which were converted to hyperfine-coupling constants by multiplication with the corresponding values for unit spin density ($A^0_{iso(P)} = 10\,200$, $A^0_{iso}(O) = -4652$ MHz), obtained from: Atkins, P. W.; Symons, M. C. R. *The Structure of Inorganic Radicals*; Elsevier: Amsterdam, 1967. This results in $A_{iso}(P) = 1081$ and $A_{iso}(O) = -41$ MHz, in good accordance with the experimental values of 1040 and −26 MHz. However, if the more recent conversion factors of Morton and Preston[19] are used ($A^0_{iso}(P) = 13\,306$ and $A^0_{iso}(O) = -5236$ MHz), the resulting couplings are significantly overestimated: 1410 and −47 MHz.

(26) Nguyen, M. T.; Ha, T.-K. *Chem. Phys.* **1989**, *131*, 245.

(27) Geoffroy, M. *Helv. Chim. Acta* **1973**, *93*, 1553.

(28) Janssen, R. A. J.; Sonnemans, M. H. W.; Buck, H. M. *J. Chem. Phys.* **1986**, *84*, 3694.

Table VII. Total Energies (au) and $\langle S^2 \rangle$ Values for $H_2\dot{P}O$ and $H_2\dot{P}OH^+$ at UHF/6-31G* and ROHF/6-31G* Levels

radical	sym	state	total energy		
			UHF	$\langle S^2 \rangle$	ROHF
$H_2\dot{P}O$	C_{2v}	$^2B_1$	−416.670699	0.7709	−416.663984
$H_2\dot{P}O$	$C_s(1)$	$^2A'$	−416.700473	0.7744	−416.694063
	$C_s(2)$	$^2A'$			−416.690191
$H_2\dot{P}OH^+$	C_1		−417.014465	0.7500	−417.012128

Table VIII. Isotropic and Dipolar Hyperfine Couplings for $H_2\dot{P}O$ and $H_2\dot{P}OH^+$ at UHF and ROHF/6-31G* Levels

radical	sym	method	nucleus	A_{iso}		$2A_{dip}$	
				au	MHz	au	MHz
$H_2\dot{P}O$	C_{2v}	UHF	^{31}P	0.2974	538	1.8031	387
			^{17}O	0.1388	−84	1.5600	−113
		ROHF	^{31}P	0.0	0	1.8650	403
			^{17}O	0.0	0	0.9936	−72
$H_2\dot{P}O$	$C_s(1)$	UHF	^{31}P	0.0992	179	0.5258	113
			^{17}O	0.1441	−87	3.1985	−231
		ROHF	^{31}P	0.0746	135	0.1554	34
			^{17}O	0.0001	0	3.3644	−242
$H_2\dot{P}O$	$C_s(2)$	ROHF	^{31}P	0.5199	942	1.5400	333
			^{17}O	0.0088	−5	0.8895	−64
$H_2\dot{P}OH^+$	C_1	UHF	^{31}P	0.7650	1384	2.3529	508
			^{17}O	0.0602	−36	0.7266	−52
			^{1}H	−0.0039	−18	0.0041	22
		ROHF	^{31}P	0.7098	1285	2.3079	499
			^{17}O	0.0045	−3	0.3981	−29
			^{1}H	0.0002	1	0.0253	13

examine the electronic structure, we performed UHF and restricted open-shell Hartree–Fock (ROHF) calculations on different $H_2\dot{P}O$ geometries, using a 6-31G* basis set.[29] Unlike the UHF theory, the ROHF procedure yields a wave function that describes a pure spin state. The isotropic and anisotropic hyperfine couplings were computed according to the spin operators:

$$A_{iso} = \left(\frac{8\pi}{3}\right) h^{-1} g_e \beta_e g_N \beta_N \langle \Psi_0 | \delta(r_N) | \Psi_0 \rangle$$

$$A_{dip}(ij) = -g_e \beta_e g_N \beta_N \left\langle \Psi_0 \left| \frac{r^2 \delta_{ij} - 3ij}{r^5} \right| \Psi_0 \right\rangle \qquad i, j = x, y, z$$

The most important results of the calculations are given in Figure 9 and Tables VII and VIII. Initially, the optimized planar (C_{2v}) and pyramidal (C_s) structures were considered (Figure 9a,b). The $^2A'$ ground state of the $C_s(1)$ geometry is energetically preferred over the $^2B_1$ ground-state configuration of the C_{2v} structure. The isotropic and dipolar ^{31}P hyperfine couplings obtained for the pyramidal $C_s(1)$ $H_2\dot{P}O$ radical (Table VIII) are substantially lower than the experimental values of the $Ar_2\dot{P}O$ radicals **1a** and **1b** (Table III). For the $C_s(1)$ structure, the odd electron is entirely localized in the valence p orbital of the oxygen atom, and consequently this species does not represent a phosphorus-centered radical. For the planar C_{2v} geometry, the calculated isotropic ^{31}P and ^{17}O hyperfine couplings are dramatically different for the two methods used. The restricted (ROHF) calculation gives zero isotropic interaction, in accordance with the fact that neither the phosphorus 3s nor the oxygen 2s atomic orbital contributes to the SOMO. The unrestricted (UHF) calculation, on the other hand, erroneously predicts a large value of $A_{iso}(P)$ of 538 MHz. Despite the modest deviation of the corresponding (S^2) value (0.7709) from the pure-spin-state eigenvalue (0.75), this result is entirely due to spin contamination! The ROHF calculation on C_{2v} $H_2\dot{P}O$ describes a phosphorus-centered radical, since the spin density is mainly confined to the

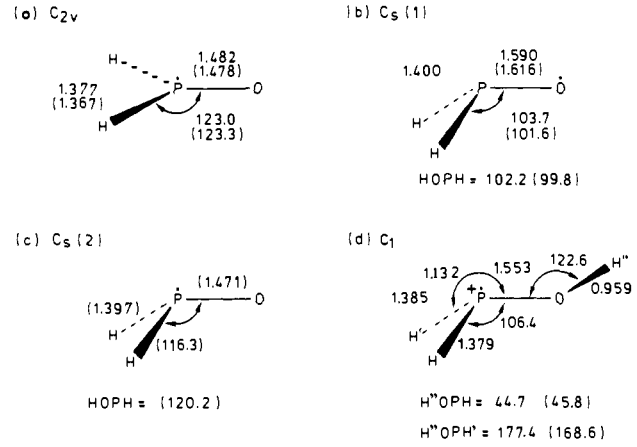

Figure 9. Optimized geometries of $H_2\dot{P}O$ and $H_2\dot{P}OH^+$ at UHF/6-31G* and ROHF/6-31G* (values in parentheses, if different from UHF values).

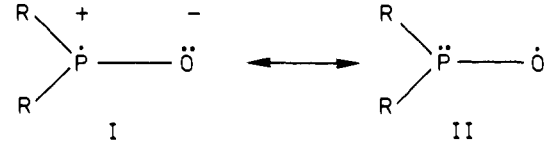

Figure 10. Canonical resonance structures of phosphoryl radicals.

valence 3p orbital of phosphorus, perpendicular to the molecular plane.

The significant difference in the calculated spin density distribution between $C_s(1)$ and C_{2v} structures must be the result of their respective geometries. Apart from being planar, the C_{2v} geometry differs from the $C_s(1)$ structure in the length of the PO bond by more than 0.1 Å. Apparently, the PO bond length is decisive for the spin density distribution. This can be rationalized by examining the two most important canonical valence-bond structures, I and II, of a phosphoryl radical (Figure 10).

For structure I, the unpaired electron is localized on phosphorus and formal positive and negative charges are associated with the phosphorus and oxygen nuclei. In structure II, there are no formal charges and the spin density is found at oxygen. A contribution of canonical structure I implies a partial separation of charge, which is electrostatically unfavorable for long PO bonds. Therefore, the calculated $C_s(1)$ configuration (PO = 1.616 Å, ROHF) is essentially an oxygen-centered radical (II), whereas the C_{2v} form (PO = 1.478 Å, ROHF) is a phosphorus-centered radical (I). To study the effect of the PO bond on the spin distribution in more detail, we optimized several C_s structures for fixed PO bond lengths ranging from 1.4 to 1.6 Å using both the UHF and ROHF formalisms. The results are summarized in Figure 11 and show a dramatic increase of $A_{iso}(P)$ and $2A_{dip}(P)$ on contracting the PO bond. Concomitantly, the HPOH dihedral angle changes from 102.2° (99.8°) at the UHF- (ROHF-)optimized geometry to 119.6° (121.0°) at PO = 1.4 Å.

There is only a modest rise in energy associated with the PO bond length reduction: a contraction of 0.2 Å requires less than 7 kcal/mol (ROHF). Much to our surprise, however, the ROHF calculations reveal a second minimum on the C_s potential energy surface ($C_s(2)$, Figure 11), which lies only 2.43 kcal/mol above $C_s(1)$ and possesses an appreciably shorter PO bond length. The isotropic and dipolar hyperfine couplings calculated for the $C_s(2)$ configuration amount to 942 and 333 MHz, respectively, and are in good agreement with experimental data on phosphoryl radicals (Tables I and III).

In this respect, it is worth mentioning that Nguyen and Ha established that optimization of $H_2\dot{P}O$ using a 6-31G** basis set at UHF and UMP2 levels results in PO bond lengths of 1.589 and 1.495 Å, respectively. Apparently, the effect of taking electron correlation into account reverses the absolute-minimum position from $C_s(1)$ toward $C_s(2)$, with respect to the UHF–SCF level.[26] The isotropic hyperfine couplings reported by Nguyen and Ha[30]

(29) Frisch, M. J.; Head-Gordon, M.; Schlegel, H. B.; Raghavachari, K.; Binkley, J. S.; Gonzalez, C.; Defrees, D. J.; Fox, D. J.; Whiteside, R. A.; Seeger, R.; Melius, C. F.; Baker, J.; Martin, R. L.; Kahn, L. R.; Stewart, J. J. P.; Fluder, E. M.; Topiol, S.; Pople, J. A. *Gaussian 88*; Gaussian, Inc.: Pittsburgh, PA, 1988.

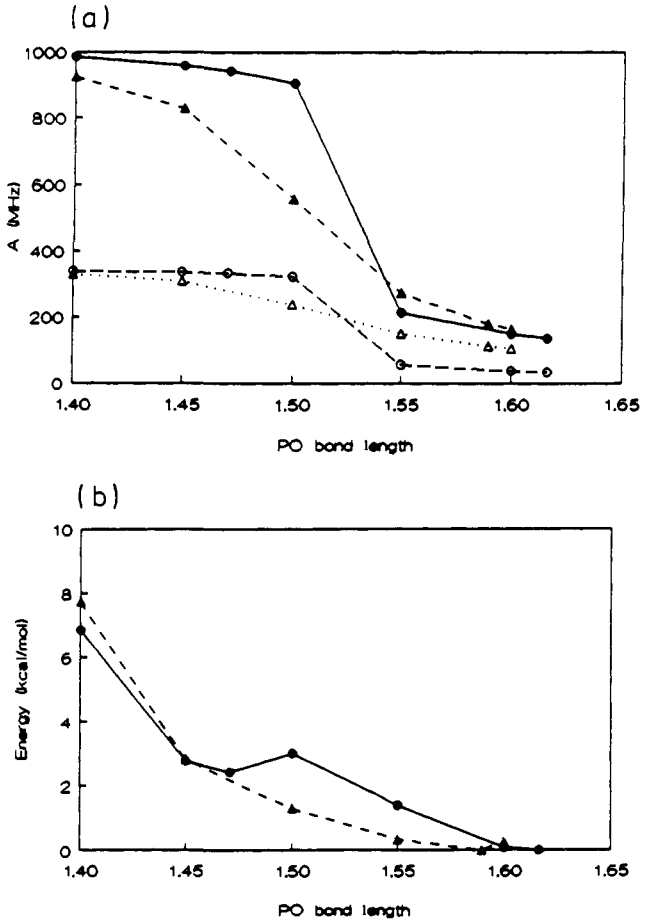

Figure 11. (a) Isotropic (filled) and dipolar (open) ^{31}P hyperfine interactions of the C_s $H_2\dot{P}O$ radical as a function of the PO bond length, calculated at UHF/6-31G* (triangles) and ROHF (circles) SCF levels. (b) Relative total energy of the C_s $H_2\dot{P}O$ radical as a function of the PO bond length, calculated at UHF (triangles) and ROHF (circles) SCF levels.

for both structures are in accordance with the present assertion that shorter PO bonds lead to higher phosphorus spin density.[30]

The reason for these strong effects of the quantum-chemical method used on the geometry and hyperfine couplings is the fact that for a range of PO bond lengths two nearby states of $H_2\dot{P}O$ exist, corresponding to the resonance structures I and II in Figure 10. The preferred geometries of the two states are significantly different. A hypothetical geometry optimization of canonical structure I results in a shorter PO bond and a smaller degree of pyramidalization compared to those of the relaxation of II, where the decreased electrostatic attraction will elongate the PO bond and the free-electron pair at phosphorus will ensure strong pyramidalization. This simple rationale is elegantly illustrated by the respective $C_s(2)$ and $C_s(1)$ minima on the ROHF energy surface.

In summary, it appears that an ROHF/6-31G* calculation can give a quantitatively correct evaluation of the isotropic and dipolar hyperfine couplings. Nevertheless, we agree with Nguyen and Ha that in this particular case high-level configuration-interaction calculations are necessary to assess the structure and electronic properties of $H_2\dot{P}O$ in depth.

Computations on $H_2\dot{P}OH^+$ as a model for radical **1c** at the UHF/6-31G* and ROHF/6-31G* levels invariably result in a phosphorus-centered species. Geometry optimization affords a nonsymmetric molecule in which the hydroxyl proton is in a transorientation with respect to one of the phosphine hydrogen nuclei (Table VII). Both isotropic and dipolar ^{31}P hyperfine interactions are large and presumably overestimated (Table VIII). In addition, the hyperfine coupling to the hydroxyl proton is small. The net effect of adding a single proton to the oxygen atom of $H_2\dot{P}O$ is thus a stabilization of resonance structure I (Figure 10), which confines the spin density to phosphorus.

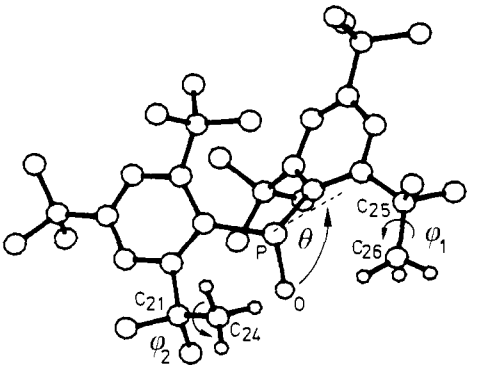

Figure 12. Initial molecular structure of the bis(2,4,6-tri-*tert*-butylphenyl)phosphoryl radical **1a**, indicating the three geometric parameters θ (PO inversion), ϕ_1 (C_{25}–C_{26} bond rotation), and ϕ_2 (C_{21}–C_{24} bond rotation) involved in the stereoinversion process.

It is our experience that calculations on isolated molecules often predict a much stronger effect of protonation that can be observed experimentally. For example, previous experiments on progressively substituted phosphoranyl radicals ($R_3\dot{P}S^-$, $R_3\dot{P}SR$, $R_3\dot{P}SR_2^+$) have shown, in contrast with quantum-chemical calculations, that the unpaired electron distribution is fairly insensitive to the number of substituents on sulfur.[31] A similar conclusion now emerges from comparison of the calculations on $H_2\dot{P}O$ and $H_2\dot{P}OH^+$ with the experiments on radicals **1a**, **1b**, and **1c**.

Van der Waals Energy Calculations. On the basis of the spin-Hamiltonian parameters, the radical structures of **1a** and **1b** are similar, though differently oriented in the crystal lattice. We have indicated that the conversion of **1a** into **1b** corresponds to a stereoinversion. The only rational explanation for the stereoinversion involves the transposition of the oxygen atom, since a reorientation of the bulky tri-*tert*-butylphenyl groups is severely hindered in the crystal lattice. It is conceivable that the space of the lost chlorine atom will be filled by the smaller oxygen atom, resulting in the inverted geometry. This description is in accordance with the directional information of the $A_3(^{31}P)$ hyperfine interaction of **1a** and **1b**.

In order to obtain an estimate of the steric energy required for the proposed inversion in the crystal, we calculated the change in van der Waals energy associated with the migration of the oxygen atom to the vacant chlorine location. For this purpose, we used the X-ray crystallographic data.[5,6] The stationary crystalline environment of the radical was formed by all neighboring atoms in 26 surrounding unit cells lying within a distance of 8 Å from the phosphoryl oxygen. The van der Waals energy was calculated from Allinger's empirical potential function:[32]

$$E_{vdW} = (\epsilon_i\epsilon_j)^{1/2}(1.84 \times 10^5 \exp(-12.0P) - 2.25P^6)$$

$$P = R_{ij}/(R_i^* + R_j^*)$$

in which ϵ_i is the energy parameter related to the depth of the potential well, R_i^* the van der Waals radius, and R_{ij} the internuclear distance.

Initially the radical geometry was taken as identical to that of the precursor molecule lacking the chlorine atom. We calculated the change in van der Waals energy (ΔE_{vdW}) in the crystal en-

(30) See Nguyen and Ha:[26] For the UHF/6-31G** optimization of a C_s structure, a PO bond of 1.589 Å is reported and $A_{iso}(P)$ = 184 MHz. For the UMP2/6-31G** calculation, the bond length is 1.495 Å, and a subsequent RCISD/DZP calculation using the UMP2/6-31G** geometry gives $A_{iso}(P)$ = 860 MHz.

(31) (a) Janssen, R. A. J.; Aagaard, O. M.; van der Woerd, M. J.; Buck, H. M. *Chem. Phys. Lett.* **1990**, *171*, 127. (b) Janssen, R. A. J.; Kingma, J. A. J. M.; Buck, H. M. *J. Am. Chem. Soc.* **1988**, *110*, 3018.

(32) For sp^2 C and H: Allinger, N. L.; Lii, J.-H. *J. Comput. Chem.* **1987**, *8*, 1146. For sp^3 C, P, and O: Allinger, N. L.; Yuh, Y. H. *MM2*, QCPE, Program 395.

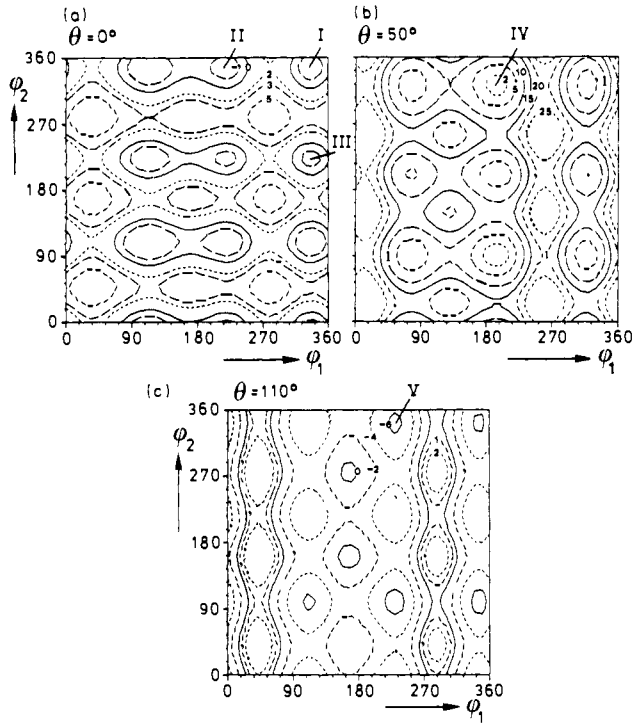

Figure 13. Contour plots of the change in van der Waals energy (kcal/mol) in the single crystal as a function of the methyl group rotations ϕ_1 and ϕ_2 for (a) the initial (θ = 0°), (b) transition-state (θ = 50°), and (c) final (θ = 110°) orientations of the PO-inversion angle. The specific points I–V are explained in the text.

countered upon migration of the PO bond toward the former PCl linkage. The preliminary calculations gave three main results. First, the calculated activation energy barrier of 28.6 kcal/mol is much too large to explain the observed inversion at 120 K. Second, there is a direct increase of the barrier when the PO vector is allowed to move out of the ClPO plane of the precursor. The third important result is the fact that the dominant contributions to the activation energy result from *intra*molecular steric interactions rather than from the surrounding molecules. Examination on atomic level reveals that severe steric hindrance is encountered with the methyl hydrogens of the ortho-*tert*-butyl carbon atoms C_{24} and C_{26} (Figure 12).

In order to avoid these close CH···O contacts, we studied the change in van der Waals energy of the phosphoryl radical (without environment) caused by PO bond migration, while simultaneously allowing for the adjustment of the methyl hydrogen positions via rotation around the C_{25}–C_{26}(ϕ_1) and C_{21}–C_{24}(ϕ_2) bonds (Figure 12). We computed the van der Waals potential energy surface for the methyl group rotations at several orientations of the PO bond (angle θ, Figure 13). It appears that for every θ value of the PO orientation nine distinct minima and maxima are predicted, which is a direct result of the rigid-rotor approximation. Figure 13 displays the contour plots for the initial geometry (θ = 0°), the transition state (θ = 50°), and the inverted configuration (θ = 110°) as a function of the two methyl group orientations ϕ_1 and ϕ_2. The calculations for θ = 0° show that the crystal structure data do not correspond to a van der Waals minimum. A small rotation to conformation I (Figure 13a, ϕ_1 = 340°, ϕ_2 = 350°) results in a lowering of the energy (ΔE_{vdW} = −1.6 kcal/mol). From this minimum, two other adjacent minimum-energy packings II and III, at coordinates ϕ_1 = 220°, ϕ_2 = 350° (ΔE_{vdW} = −1.6 kcal/mol) and ϕ_1 = 340°, ϕ_2 = 220° (ΔE_{vdW} = −1.4 kcal/mol) can be reached via low-energy transition states of ΔE_{vdW} = 1.9 kcal/mol and ΔE_{vdW} = 3.5 kcal/mol, respectively. In contrast to migration of the oxygen atom at ϕ_1 = ϕ_2 = 0°, the transposition of the PO vector from the minimum at ϕ_1 = 220°, ϕ_2 = 350° is a low-energy process with a transition state of ΔE_{vdW} = 1.1 kcal/mol at θ = 50°, ϕ_1 = 200°, ϕ_2 = 320° (IV in Figure 13b). In addition, the final inverted geometry at θ = 110°, ϕ_1 = 230°, ϕ_2 = 340° possesses a ΔE_{vdW} value of −6.3 kcal/mol (V in Figure 13c). The latter value confirms the experimental result that the conversion of **1a** into **1b** is a unidirectional process. The results remain essentially unaltered when surrounding molecules are included in the calculation, which demonstrates the *intra*molecular nature of the reaction. A release of the PO vector out of the ClPO plane of the radical precursor immediately leads to high ΔE_{vdW} energies for all values of θ, ϕ_1, and ϕ_2. A shortening of the PO bond of 5% shifts the total energy surface to a lower value by approximately 0.2 kcal/mol, hardly affecting the relative energies.

In summary, it appears that the inversion will probably occur via a coupled motion of the PO bond vector and the two ortho-*tert*-butyl methyl groups. Perhaps, even more synchronous motions are involved. The simplification made in the present computational model prohibits a quantitative assessment of the actual activation barrier. However, our calculations are in qualitative agreement with the experimental results and provide insight into the geometry relaxations which might occur.

Conclusion

The present study shows that the chiral phosphoryl radical **1a**, formed from bis(2,4,6-tri-*tert*-butylphenyl)phosphinic chloride by a dissociative electron-capture reaction, exhibits an enantioselective stereoinversion at approximately 120 K into its isomer **1b**. This result was obtained via a single-crystal ESR study, which affords directional information on the orientation of the SOMO. In combination with X-ray crystallographic data, a detailed description of the radical geometries of the two isomers **1a** and **1b** could be obtained. Packing energy calculations show that the stereoinversion occurs in a coupled rotation of the phosphoryl oxygen and two methyl groups of the ortho *tert*-butyl substituents. The process is entirely controlled via *intra*molecular steric interactions. The surrounding molecules are only involved in confining the 2,4,6-tri-*tert*-butylphenyl groups in their predefined crystallographic spatial structure. Van der Waals energy calculations confirm the experimental result that the stereoinversion is a unidirectional process by the fact that the steric energy in the crystal is reduced when the phosphoryl oxygen is transferred to the more spacious vacant chlorine location. There is evidence for a secondary reaction in which the inverted structure **1b** abstracts a proton from a *tert*-butyl group, leading to the protonated phosphoryl radical **1c**.

Acknowledgment. This investigation has been supported by the Netherlands Foundation for Chemical Research (SON) with financial aid from the Netherlands Organization for Scientific Research (NWO). We thank Dr. J. A. Kanters and Mr. A. Schouten (State University of Utrecht, The Netherlands) for the redetermination of the cell parameters. Professor M. Yoshifuji (Tohoku University, Sendai, Japan) is gratefully acknowledged for providing the crystallographic atomic coordinates of bis-(2,4,6-tri-*tert*-butylphenyl)phosphinic chloride.

Registry No. 1, 73557-52-5; **1a**, 83408-22-4; $H_2P^{\bullet}O$, 97516-21-7.

Supplementary Material Available: A textual presentation of the synthesis, NMR spectra, and elemental analysis of compound **1** (1 page). Ordering information is given on any current masthead page.